7-1-2016

The DarkLight Rises: Visible Light Communication in the Dark

Zhao Tian
Dartmouth College

Kevin Wright
Dartmouth College

Xia Zhou
Dartmouth College

The DarkLight Rises: Visible Light Communication in the Dark

Dartmouth Computer Science Technical Report TR2016-814

Zhao Tian, Kevin Wright†, and Xia Zhou
Department of Computer Science, Department of Physics and Astronomy†
Dartmouth College, Hanover, NH
{tianzhao, xia}@cs.dartmouth.edu, kevin.wright@dartmouth.edu

ABSTRACT

Visible Light Communication (VLC) emerges as a new wireless communication technology with appealing benefits not present in radio communication. However, current VLC designs commonly require LED lights to emit shining light beams, which greatly limits the applicable scenarios of VLC (e.g., in a sunny day when indoor lighting is not needed). It also entails high energy overhead and unpleasant visual experiences for mobile devices to transmit data using VLC. We design and develop DarkLight, a new VLC primitive that allows light-based communication to be sustained even when LEDs emit extremely-low luminance. The key idea is to encode data into ultra-short, imperceptible light pulses. We tackle challenges in circuit designs, data encoding/decoding schemes, and DarkLight networking, to efficiently generate and reliably detect ultra-short light pulses using off-the-shelf, low-cost LEDs and photodiodes. Our DarkLight prototype supports 1.3-m distance with 1.6-Kbps data rate. By loosening up VLC's reliance on visible light beams, DarkLight presents an unconventional direction of VLC design and fundamentally broadens VLC's application scenarios.

CCS Concepts

•**Networks** → **Wireless access networks;**

Keywords

Visible light communication; Energy efficiency; Random access control

1. INTRODUCTION

The idea of reusing ubiquitous lights around us for data communication is intriguing. Empowered by Visible Light Communication (VLC) [21, 34], ceiling LED lights serve as wireless access points that provide network connectivity to smart devices (e.g., smartphones) in a room. Exploiting light as a new communication modality, VLC offers 10K times greater bandwidth than radio spectrum, allows highly dense concurrent links because of its directionality, and more importantly, ensures better security/privacy by confining communication within a room since light cannot penetrate walls. A key appealing benefit of VLC is that it is built upon existing lighting infrastructure. It adds data communication as an additional functionality of lights and requires minimal deployment overhead (only attaching a low-cost modulation unit to existing LED lights).

But what happens to data communication when LED lights appear off or dark? As the conventional wisdom goes, communication is no longer sustained. Indeed, existing research on VLC has commonly taken it for granted that light beams are visibly present during data communication. The tight reliance on visible light beams brings two problems in practical scenarios. *First*, in fact, there are a large number of scenarios where we desire minimal or no indoor lighting (e.g., in a sunny day with bright sunlight leaking through the window, or in the night during our sleep), while our smart devices still demand network connectivity to chirp out small amount of data (e.g., smart thermostats sending temperature data, smart phones staying connected to the Internet for email updates). Current VLC designs fail to maintain communication in these scenarios. *Second*, when VLC is brought to the world of mobile devices, the reliance on visible light beams not only creates visually unpleasant experiences to users carrying or wearing these devices, but also entails prohibitive energy overhead for mobile devices to transmit data using VLC. Even the low-power LEDs of today's smartphones consume up to 900 mW [3]. Keeping the LED on quickly drains the device battery. Recent work [37] aims to address this problem by reflecting incoming light beams to transmit data. However, it still requires shining light beams from the ceiling and the reflected light beams remain visually unpleasant to users.

In this paper, we seek to loosen up VLC's reliance on visible light beams and sustain data communication even when the LED emits extremely-low luminance. To this end, we propose *DarkLight*, a new VLC primitive that maintains the light-based communication even if the light appears dark or off. The key idea is to encode data into ultra-short light pulses at a high frequency, such that these light pulses are imperceptible to human eyes yet detectable by photodiodes. Any devices equipped with photodiodes can sense the changes in the light pulses and decode data. DarkLight broadens the applicable scenario of VLC, as it serves as a special mode that a VLC link can seamlessly switch to whenever perceptible light beams are not desired (e.g., in a sunny day). Thus, when integrated with VLC's normal mode where LEDs are visually on, DarkLight allows light-based communication be always-on, regardless of the actual light luminance. Furthermore, with the LED light operating on an ultra-low duty cycle, DarkLight significantly drives down the energy consumption of the LED front end and thus makes VLC more affordable to mobile devices with tight energy budget.

To realize DarkLight in practice, we face three challenges. *First*, it is non-trivial to generate and detect such ultra-short light pulses using off-the-shelf LEDs and photodiodes. Because of their limited response time and ultra-short pulse duration, the resulting light pulses have not yet reached the peak light intensity of the LED, limiting the communication distance. *Second*, these ultra-short, sparse light pulses impose challenges on the modulation and demodulation design. Common VLC modulation schemes either fail to keep light pulses imperceptible (e.g., PWM [21]), or lead to very low data rates (e.g., 40 bps) tightly constrained by the ultra-low LED duty cycle. Furthermore, these fragile, ultra-short light pulses are

susceptible to ambient light fluctuations, causing decoding errors. *Finally*, in a DarkLight network, a DarkLight receiver can perceive light pulses from multiple transmitters. These light pulses can collide at the receiver and cause decoding errors.

We develop a holistic solution including circuit, systems designs and analytical studies to tackle the above challenges. *First*, we compensate the limited sensitivity of off-the-shelf LEDs and photodiodes with effective driving circuit designs that react sufficiently fast (in nanoseconds) for minimal delay and boost the gain of low-cost photodiodes to improve communication distance. *Second*, given the ultra-low LED duty cycle, we apply a lightweight yet efficient modulation scheme to maximize the number of bits encoded into each single ultra-short light pulse. We also develop robust demodulation scheme to extract bits reliably from light pulses. *Third*, we further boost the data rate by exploiting the difference of human visual perception in different ambient light conditions. We subtly adapt the LED duty cycle to current ambient light level, which greatly improves the link rate and yet still maintains the resulting luminance imperceptible. *Finally*, we extend to a network of DarkLight links, allowing a DarkLight receiver to decode bits from multiple LEDs simultaneously and fine-tuning single link configuration based on analytical results of collision probability.

DarkLight Prototype. We develop a DarkLight prototype, using off-the-shelf, low-cost LEDs (Cree CXA, $7) and photodiodes (Honeywell SD5421, OPT101, $6 - $8). We have systematically examined both its user perception and system performance. Our key findings are as follows:

- With 500-ns light pulses and 0.007% LED duty cycle, a DarkLight LED is indistinguishable from an LED in light-off mode, when users perceive the illuminance on environmental objects in different ambient light conditions;
- DarkLight achieves 1.6 Kbps data rate and supports up to 1.3 m communication distance;
- DarkLight drastically reduces the power consumption of the LED front end from 19.8 W to 104 μW and operates with low-power driving circuits ($<$ 48 mW for the transmitter and $<$ 50 mW for the receiver);
- A DarkLight receiver effectively resolves local conflict and receives data from multiple LED transmitters simultaneously. Its throughput scales almost linearly as the number of perceived LEDs grows.

We greatly advance prior work [48] by boosting the supporting distance from 10 cm to 1.3 m with more sophisticated circuit and system designs. We also systematically study the network of DarkLight links to optimize networkwide performance. Another related work [17] has discussed the standard for lights to appear off and simulated resulting data rates. Our work goes beyond analytical results and simulations by designing and implementing a practical system realizing light-based communication in the dark.

Comparison to RF and Infrared. Radio frequency (RF) and infrared (IR) are alternative communication frequencies that are intrinsically imperceptible. Operating on the visible light spectrum, DarkLight complements them and offers its unique benefits. Compared to RF, DarkLight achieves better security by confining communication within a room as light cannot penetrate the wall. Compared to IR, DarkLight is safer. Prior studies [33, 31] have shown that IR can cause eye safety issues with high power and long exposure time [31]. Specifically, for IR rays with wavelength between 780 and 950 nm (used in IR communication), they can pass through the human cornea and be focused by the lens onto the retina, potentially inducing thermal damage [33]. The principle of DarkLight is in fact general and can be applied to IR to lower its power while maintaining IR communication. Furthermore, IR emitters are not universally available on mobile devices, while cameras, or flashlights, or LED indicators are the norm for mobile devices. DarkLight offers an additional option when IR is not available.

Contributions & Applications. DarkLight sets a new paradigm of light-based communication. It presents a departure from the conventional VLC and fundamentally broadens the application scenarios of VLC. Our work identifies and tackles key systems challenges to realize DarkLight using off-the-shelf, low-cost devices. It also generates far-reaching impact on provoking new ideas on VLC applications. Examples include: 1) visible light sensing [39, 40, 59], which reuses light rays to sense user behaviors. It requires always-on connectivity and yet does not require high data rates. DarkLight can enable 24/7 visible light sensing even when the illumination of LEDs is not needed; 2) wireless authentication reusing built-in LEDs and light sensors on mobile devices. Because of its energy efficiency and high directionality, DarkLight is preferable to its RF alternatives; and 3) connecting smart devices as part of the open web of things [7, 53].

2. CONCEPT AND CHALLENGES

To enable light communication even if light beams are not visually seen, DarkLight exploits the difference between human eye perception and the responsiveness of photodiodes. Next we first overview the concept of DarkLight and then describe the practical challenges to realize the concept.

DarkLight Concept. The capability of human eyes perceiving visible light differs drastically from that of photodiodes. Our eyes perceive light through photoreceptors [20], a specific type of neuron in the retina, which convert light into signals that can stimulate visual perception. Specifically, they absorb photons and trigger change in the cell's membrane potential. The effect of absorbing a photon lasts 100 ms (for rods) or 10 – 15 ms (for cones). The effects of all photons that are absorbed within a time threshold are added up, which is called temporal summation [20]. In comparison, light sensors, e.g. photodiodes, also convert light into electrical signals, but the lag time of the conversion is far shorter than visual perception. The response time of photodiodes can reach sub-microsecond.

Exploiting the difference in the response time of human eyes and photodiodes, DarkLight encodes data into ultra-short light pulses that stimulate minimal visual perception to human eyes and yet are detectable using off-the-shelf, low-cost photodiodes. These ultra-short light pulses can be generated by reducing an LED light's duty cycle, which is the percentage of the ON duration t_{ON} in a period t_{period}, $d = t_{\text{ON}}/t_{\text{period}}$. Although lowering the LED's peak light intensity during its ON state can also decrease the resulting luminance and produce imperceptible light beams, it curtails the communication distance as light luminance degrades over the square of the distance [23]. Thus, to minimize the negative impact on the communication distance, DarkLight tunes only LED's duty cycle without adjusting its peak intensity.

Practical Challenges. To realize DarkLight using off-the-shelf, low-cost LEDs and photodiodes, we face following challenges. First, generating and detecting such ultra-short, high-intensity light pulses is non-trivial, because off-the-shelf LEDs and photodiodes are limited in their sensitivity. On the LED side, off-the-shelf LED chips do not transition from OFF to ON state instantaneously. The resulting delay for an LED chip to ascend to its peak intensity is referred to as its *rise time*, which is determined by the LED's junction capacitance and its driving circuit. If the rise time is much longer

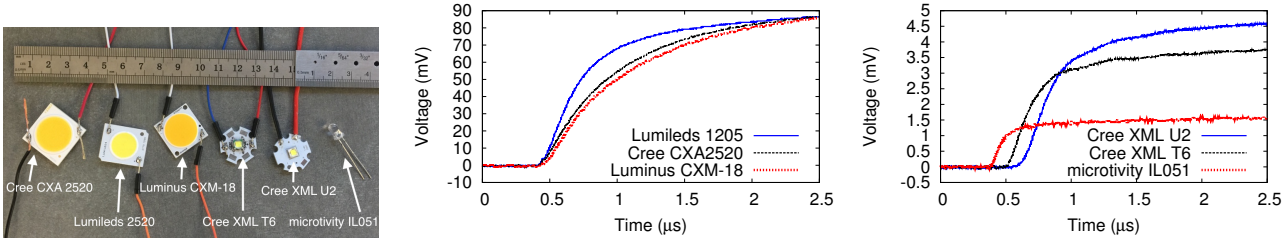

(a) Off-the-shelf LEDs (b) Rise time of high-power LEDs (c) Rise time of low-power LEDs

Figure 1: High-power and low-power, off-the-shelf LEDs and their rise times (i.e., the time to ascend to the peak light intensity).

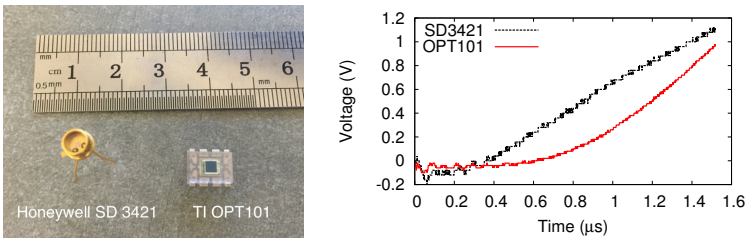

(a) Low-cost photodiodes (b) Response delay

Figure 2: Two representative low-cost photodiodes and their delay in responding to incoming light changes.

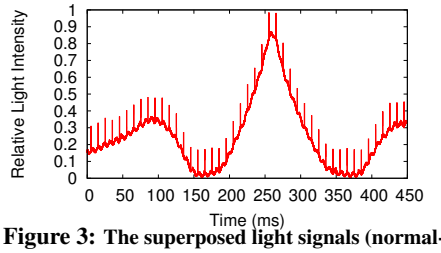

Figure 3: The superposed light signals (normalized to the maximal light intensity) received by the photodiode. The ultra-short light pulses can be buried in ambient light fluctuations.

than the light pulse duration, then the LED cannot reach its peak intensity, which can fundamentally limit the distance for photodiodes to detect light pulses. To quantitatively examine the rise times of existing LEDs, we have tested six representative types of LEDs (Figure 1(a)) on the market, ranging from three low-power LEDs with input voltage of 3.3 V to three high-power LEDs with input voltage of 36 V. For each LED, we connect it to a MOSFET to switch it and measure its rise time using a high-end light sensor (Thorlabs PDA10A) and an oscilloscope. Figure 1(b)(c) plot the output voltage of PDA10A over time, where the voltage reflects the actual luminance from each LED. We observe that it takes roughly 1 μs for high-power LEDs to rise to their 90% peak intensity and 500 – 800 ns for low-power LEDs.[1] Although low-power LEDs react faster, their peak luminance is only roughly 5% of that of high-power LEDs. Therefore, given the ultra-short pulse duration (e.g., 500 ns used in DarkLight), the resulting light pulses have a low peak, presenting challenges in their detection.

On the photodiode side, detecting ultra-short light pulses at reasonable distances (e.g., 1 m) requires photodiodes that have sufficiently high gains to support long communication distance and a short response delay not to miss ultra-short light pulses. However, our experiments show that existing low-cost ($<$ \$6) photodiodes do not satisfy both criteria. Take two types of photodiodes (OPT101 [50] and Honeywell SD3421) as examples. For each photodiode, we connect it to a 100-kΩ resistor for the same amplification factor. As shown in Figure 2, OPT101 has a higher gain but it takes 800 ns for the sensor to react to light intensity change, meaning that light pulses shorter than 800 ns cannot be detected. On the other hand, the delay of SD3421 is much shorter ($<$ 200 ns) and yet its gain is only 10% of OPT101 dictating a short communication distance. Photodiodes with high gain and fast speed, e.g. avalanche photodiodes, need high reverse voltage ($>$ 100 V) not applicable for mobile devices.

Second, the ultra-low LED duty cycle imposes challenges to the modulation and demodulation design. Common modulation designs either cannot keep the light pulses imperceptible by encoding data into changes of LED duty cycle (e.g., PWM [21]), or result into very low data rates. As an example, for the LED to produce only 0.07 lx illuminance (similar to a room at night with all lights off) at 1-m distance, the LED duty cycle needs to be below 0.0018%. Simply using the On-Off Keying (OOK) modulation [43, 51] results in only 40-bps data rate. With Frequency-Shift Keying (FSK) [38] the data rate is much lower since it requires multiple light pulses to encode data.

When it comes to demodulation, the sparse, short light pulses are vulnerable to ambient light fluctuations, which can be caused by switching on/off another light, a camera flash, or even a floating patch of cloud that covers the sun. These ambient light fluctuations can overwhelm the short light pulses, preventing photodiodes from extracting encoded light pulses from the received superposed light signals. Figure 3 shows an example of the light signals received at a photodiode (Honeywell SD5421) 1.5 m away from the LED emitting 800-ns light pulses, while a smartphone with a flashing LED as the interfering light source is swinging by.

Finally, in the presence of multiple DarkLight links, light pulses from different LEDs can collide at the a photodiode, which causes decoding errors. The fact that LEDs are incoherent devices [21] means that we cannot obtain the phase information to differentiate transmitters. Separating light pulses on the frequency domain as shown in prior works [39, 35] is also not applicable because of the encoding inefficiency of FSK in the context of DarkLight. We need to seek effective mechanisms for the receiver to decode data from multiple transmitters.

To address the above challenges, we next present our DarkLight design for a single link (§ 3), followed by the solution and analysis for dealing with multiple transmitters in a DarkLight network (§ 4).

[1]High-power LEDs reacts more slowly because they consist of integrated LED arrays with larger area, resulting into higher junction capacitance and thus longer rise time and higher luminance [36].

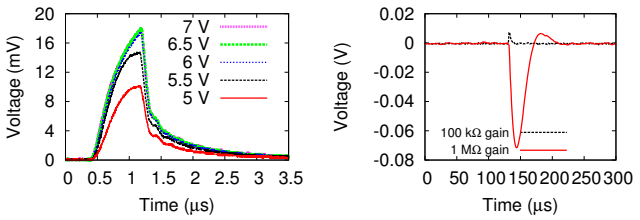

(a) Impact of gate voltage V_{cc} (b) Receiver gain improvement

Figure 4: Driving circuit design.

3. DarkLight DESIGN

We design DarkLight with the practical constraints of off-the-shelf LEDs and low-cost photodiodes in mind. By removing the need of specialized LED luminaire and high-end photododiodes that are costly and not widely deployed, we push the DarkLight design to the maximal efficiency and lower the practical barrier for DarkLight to be adopted in practice. The same DarkLight design can be applied to specialized LED and photodiodes with shorter rise/response time, achieving superior performance.

Specifically, from a single link's point of view, our design goal is to maximize the link data rate while minimizing the resulting luminance to keep light pulses imperceptible to human eyes. At the high level, DarkLight design consists of three core components: 1) effective driving circuit design to generate and detect ultra-short light pulses, 2) efficient and robust modulation/demodulation scheme, and 3) subtle adaptation of LED duty cycle to the ambient light to further boost data rate. Next, we discuss each component in detail.

3.1 Effective Driving Circuit Design

The goal of the driving circuit design is two-fold. On the LED side, we aim to allow the circuit to react super fast (in nanoseconds) to facilitate the generation of light pulses, which last only hundreds of nanoseconds. On the photodiode side, we aim to improve the photodiode gain to support reasonable communication distance.

LED Driving Circuit. Prior VLC system designs [35, 39] commonly use a MOSFET to switch the LED and a micro-controller (e.g. Arduino) to directly drive the gate of the MOSFET. However, to drive MOSFET's gate quickly, its gate capacitance needs high voltage (e.g., at least 6 V for STF5N52U, a fast power MOSFET with 13.6 ns rise time, 2.25 V beyond its threshold voltage) and high dynamic charging current (hundreds of mA or even amperes [28]), far exceeding the limited output of common micro-controllers (e.g., Arduino UNO outputs 3.3 V or 5V and 20 mA).

To overcome this problem, we combine a MOSFET with a MOSFET gate driver to boost the voltage and charging current to the MOSFET (see Figure 8). The gate voltage V_{cc} plays an important role in determining the ascending speed of LED's light intensity. To identify the proper V_{cc} value, we test different gate voltages using an off-the-shelf LED (CREE CXA 2520), and measure LED's light intensity using a high-end light sensor (Thorlabs PDA10A) placed 5 cm away. We use an FPGA to generate 800-ns square pulses for the gate driver and plot the PDA10A output voltage in Figure 4(a). We observe that higher V_{cc} leads to quicker ascending of light intensity and yet the speed improvement is marginal once V_{cc} is above 6 V. Thus we set V_{cc} to 6 V in our implementation.

Photodiode Driving Circuit. To detect ultra-short light pulses, we need photodiodes with low response delay. However, as shown in § 2, such low-cost photodiodes commonly have a low gain, greatly limiting the communication distance. We overcome this problem by judiciously designing the photodiode's amplifying circuit to boost its gain (see Figure 8). In particular, we use a transimpedance amplifier together with a feedback resistor (R_f) that determines the amplifier's gain. We use a resistor with a high resistance value (1 MΩ) to increase the receiver gain and thus the communication distance. We also add a low pass filter to reduce circuit noise [22, 24]. Figure 4(b) shows the improvement in the receiver gain with our circuit design.

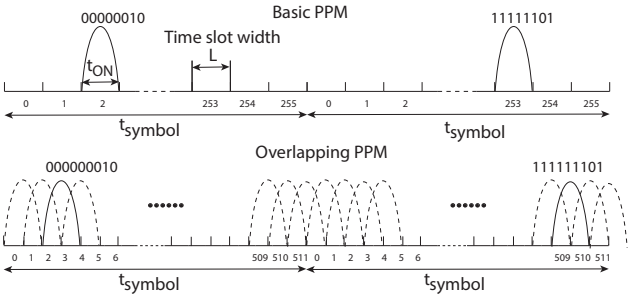

Figure 5: Pulse Position Modulation (PPM) and Overlapping PPM (OPPM). A light pulse occurs only once per symbol. Each symbol is divided into 256 time slots, thus the time slot where the light pulse resides represents 8-bit information.

3.2 From Pulses to Bits

Given these ultra-short light pulses, we now examine how to efficiently encode data into these pulses, and more importantly, reliably decode data in the presence of ambient light fluctuation.

Modulation. The sparsity of light pulses imposes a hard constraint on the encoding efficiency. To boost encoding efficiency, we choose to encode bits into the exact starting point (rise edge) of a light pulse in the time domain, which is referred to as the Overlapping Pulse Position Modulation (OPPM) [13]. As an advanced variant of PPM [21], OPPM further increases the number of bits represented by each pulse. Specifically, we divide time into symbols with equal length, where only a single light pulse occurs within a symbol. Each symbol is further divided into 2^M time slots. Thus, the exact time slot where the light pulse first occurs represents M bits. OPPM differs from PPM in the configuration of time slot width L. PPM sets L no shorter than the pulse width, while OPPM allows L to be shorter than the pulse, leading to a larger number of time slots within a symbol and thus more bits encoded by a pulse (Figure 5). The rationale is that only the starting point (rising edge) of a pulse is needed to convey the pulse position and represent bits.

Clearly the time slot width L is a key parameter in OPPM. Its configuration faces a tradeoff. A smaller L allows a finer-grained partition of a symbol, packing more bits into a pulse.[2] On the other hand, a smaller L is more prone to slot synchronization offset and collision with pulses of other DarkLight links. In § 4.2, we will discuss the configuration of L for different optimization goals in a DarkLight network.

Demodulation. To extract data out of these sparse, ultra-short light pulses, a straightforward method is maximum likelihood decoding [23], where we identify the slot with the highest received light intensity. However, in the presence of ambient light fluctuation, this method can easily end up with locating pulses incorrectly, as shown in Figure 3.

To achieve robust decoding, we leverage the fact that ambient

[2]The minimal L is determined by the ADC sampling rate, which specifies the minimal time interval between adjacent samples.

light fluctuates at a much lower speed than the generated light pulses in DarkLight. Thus, we base the pulse detection on the speed of light intensity changes, i.e., the first-order derivatives of the light signals. Simply computing the finite difference (difference between adjacent samples), however, does not accurately capture the derivatives of the underlying signal, because finite difference responds strongly to noise. To address this problem, we leverage Gaussian derivative [46], a standard edge detection technique used in computer vision. It naturally smooths the signal and computes the first-order derivatives more accurately. Specifically, we compute the first-order derivative of a Gaussian function, sample the derivative function, and use the samples as a filter to convolute with the light intensity signals. There are two important parameters in the Gaussian derivative filter: the filter size and the standard deviation (σ) of the Gaussian function. In our prototype, we set the filter length as five and choose $\sigma = 1$.

Furthermore, the decoding robustness also highly relies on accurate slot alignment. To minimize the slot offset, we insert a preamble before every data packet. The preamble consists of three symbols, each with a light pulse starting in the first time slot. This special preamble pattern is used by the receiver to detect the beginning of a packet, identify the number of slots in each symbol configured by the transmitter, and align subsequent time slots. Even though the symbol number is only 3, the corresponding bit number is around 30. The probability of misdetection is less than 10^{-6} if we assume random data. When receiver's ADC misses sample data points, it creates accumulating errors and causes decoding errors of later pulses. To address this problem, each time we detect a rise edge, we identify the time slot the rise edge belongs to, realign the slot to the rise edge, and shift subsequent samples correspondingly.

3.3 Adapting to Ambient Light

Finally, we exploit the impact of ambient light on human vision perception to further boost the data rate of a single DarkLight link. Currently the ultra-low duty cycle d (e.g., 0.007%) is the ultimate limiting factor of DarkLight's data rate, which can be calculated as $d \cdot M/t_{ON}$, where each light pulse represents M bits and t_{ON} is the pulse width. We seek to adapt LED's duty cycle to ambient light while maintaining light pulses imperceptible. The rationale is that human eyes are more sensitive to light in a dark environment than in a bright condition.[3] Based on this rationale, we can increase the LED's duty cycle when ambient light is stronger while keeping light pulses from the LED imperceptible. Such adaptation of the LED duty cycle helps further raise the data rate, since indoor ambient brightness varies greatly within a day, e.g., the illuminance of a room can exceed 2000 lx in a sunny day. We next describe the key steps to enable adaptation.

Sensing the Ambient Light. To achieve automatic adaptation, transmitters (LEDs) should be able to sense and measure the ambient light intensity. There are two available methods: 1) using the LED itself as a light sensor [50, 43], given that an LED has a similar structure as a photodiode and can also convert photons to electrical current; 2) adding a photodiode alongside the LED chip [37]. Although the first method conceptually has a cleaner setup, it entails two practical limitations. First, an LED is half-duplex and thus has to switch between sensing and transmission. The switching incurs delay in milliseconds, limiting the sensing frequency. Second, to enable LED sensing, we need additional circuit components to isolate the LED driver circuit and amplifier circuit, so that they do not affect each other. It adds control complexity and the isolators consume additional power. Thus, in DarkLight, we choose to add a photodiode alongside the LED. It presents no limits on sensing frequency, simplifies the overall circuit, and lowers the driving circuit energy consumption. To mitigate the photodiode saturation problem, we connect a small feedback resistor in the transimpedance amplifier to form a low-gain receiver (see Figure 8). It allows the transmitter to sense a wide range of indoor ambient light illuminance change (e.g., 10^{-1} – 2000 lx).

Adapting the LED Duty Cycle. Based on the sensed ambient light condition, DarkLight adapts its LED duty cycle using a lookup table. We divide ambient light intensity into K levels and map each ambient light level $i(\in [1, K])$ to a LED duty cycle d_i, such that d_i is the maximal LED duty cycle that keeps the resulting luminance imperceptible to human eyes under the ambient light level i. We build this mapping table through extensive study on user perception (see § 6.1) and store this mapping as a lookup table (Table 1). The transmitter periodically senses the ambient light. Once the ambient light changes across levels, the transmitter then searches through the lookup table to identify the new duty cycle, and adapts accordingly by adjusting the number of slots. Note that we keep the pulse width the same because the change of pulse width changes the communication distance.

Implications on Demodulation. With the adaptation described above, the slot number in each symbol, a key parameter used in decoding, can vary. To ensure correct decoding under varying LED duty cycles, the receiver examines the preamble pattern to identify the current duty cycle used by the LED. Specifically, since the first two light pulses in the preamble are both located in the first slot of a symbol, the time interval between these two pulses is the symbol length. Dividing it by the slot width configured in § 4.2 gives the number of slots in each symbol. An alternative approach is to let the DarkLight receiver also sense the ambient brightness and search through the same lookup table to obtain the current duty cycle. This, however, requires the receiver to calibrate with the photodiode at the transmitter. Furthermore, the transmitter and receiver can perceive different ambient light because of the non-uniform illuminance distribution in a room caused by shadowing.

4. NETWORKING DarkLight

We now move on to a network of DarkLight links, seeking to optimize networkwide performance. Operating on the visible light spectrum, a DarkLight link is inherently directional. However, given the receiver photodiode's field-of-vision (FoV) and LED density, a DarkLight receiver can still likely perceive light pulses from multiple LEDs. Light pulses from multiple LED sources confuse receiver's decoding. They can also overlap and cause decoding errors. Enforcing link access control is challenging for ceiling LEDs, given that LEDs all face downwards and cannot sense one another's light rays. Other alternative methods include time-division multiaccess (TDMA) control and retransmission upon each collision. However, they greatly sacrifice network throughput.

To address this problem, we develop a mechanism for a DarkLight receiver to separate ultra-short light pulses from different LEDs and decode bits from multiple LEDs simultaneously. Compared to TDMA or retransmission-only methods, it not only boosts a single receiver's throughput (especially helpful for ceiling LEDs transmitting heavy downlink traffic), but also removes the need to tightly synchronize all LEDs, which can be tricky given the diverse light sources (e.g., LEDs on mobile devices, ceiling LEDs, floor lamps, table lamps, wall lamps, etc) in an environment. Further-

[3]The physiologic explanation is that our retina contains two light-sensitive cells: rod and cone cells. Rods are more sensitive than cones and only mediate our vision at low ambient light levels [42], making eyes more sensitive to light when ambient light is darker.

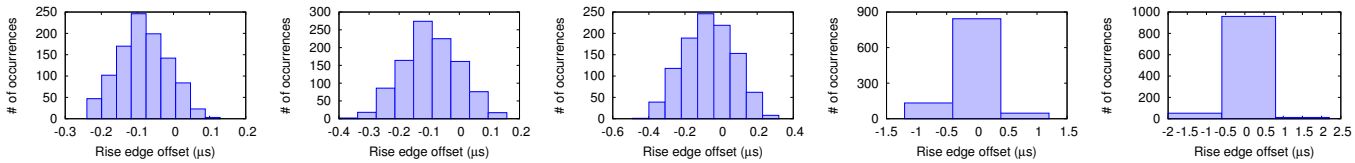

(a) 7.14 MHz (b) 4.76 MHz (c) 3.03 MHz (d) 1 MHz (e) 500 KHz

Figure 6: The distribution of rise edge offset (i.e., time difference between the start of a rise edge and the start of its nearest time slot) observed by the DarkLight receiver (Honeywell SD5421 photodiode), under varying sampling rates.

more, to support visible light sensing, it is crucial for a receiver to perceive lights from multiple LEDs concurrently.

Next we describe our mechanism to embrace multiple transmitters, followed by collision analysis and single link configuration for optimal networkwide performance.

4.1 Embracing Multiple Transmitters

We aim to allow a receiver to decode bits from light pulses emitted by multiple LEDs simultaneously. Our solution is driven by a simple observation: each LED has its own set of time slots for data encoding, and the rise edges of light pulses from this LED only appear at the beginning of this LED's time slots. Thus, if a rise edge does not align with the beginning of any slot of this LED, the associated light pulse does not come from this LED. We can then differentiate multiple simultaneous bit streams from different LEDs, as long as their slots do not align perfectly. Next we first examine the actual rise edge offset (i.e., the offset from the start point of its nearest time slot) observed by the receiver, followed by the detail of separating pulses from different LEDs.

Quantifying Rise Edge Offset. The transmitter aligns the rise edges of light pulses perfectly with the beginning of its slots. The receiver, however, can observe offsets because of hardware artifacts. To understand the offset magnitude, we conduct experiments as follows. We instrument the transmitter to send 1024 random OPPM symbols (with 256 slots each). We then sample the light signals with different rates, ranging from 500 KHz to 7.14 MHz. We use the edge detection method in § 3.2 to locate each rise edge, compute the time difference between adjacent rise edges, and derive the time offset as the remainder with a modulus of the time slot width L. We calculate the time difference with respect to the previous rise edge instead of the first rise edge to avoid the impact of sampling rate inaccuracy.

Figure 6 plots the offset histogram under different sampling rate. Our key observation is that rise edge offsets are much smaller (within 2 μs) than the received pulse width (40 μs) and exhibit roughly a zero-mean Gaussian distribution with a very small variance. The mean is not a perfect zero because the ADC sampling rate is imperfect (artifacts of crystal oscillators). Given that we use the sampling rate to calculate the time difference, when the actual sampling rate is smaller than the nominal sampling rate, the calculated time is underestimated. We can push the mean offset closer to 0 by calibrating the ADC sampling rate. In addition, lower sampling rates lead to slightly larger offsets. The reason is that we locate the rise edge by finding the point with the largest derivative, which means the light signal ascends fastest at this point. With a lower sampling rate, ADC is more likely to miss this point during sampling.

In conclusion, we can experimentally decide the range θ of the possible rise edge offset, $[\underline{\theta}, \bar{\theta}]$, where $\theta = \bar{\theta} - \underline{\theta}$, and use it to determine whether a pulse is emitted from an LED. For example, for the sampling rate of 1 MS/s, we can set $\underline{\theta} = -1.5$ μs and $\bar{\theta} = 1.5$ μs.

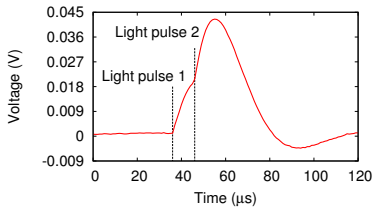

Figure 7: Rise edges of two light pulses overlap at a RX photodiode.

Identifying Pulse Sources. We refer to the encoded light pulses from a LED as a *stream*. The DarkLight receiver continuously senses incoming light intensity, identifies pulses' rise edges, and assigns each rise edge to a stream. Specifically, as shown in Algorithm 1, for a pulse with rise edge starting at t, the receiver computes the interval between t and the most recent rise edge of each known stream i, and derives the rise edge slot offset q_i. This pulse belongs to stream i if only q_i is within the rise edge offset range (i.e., $\underline{\theta} < q_i < \bar{\theta}$). If no such stream is found, this rise edge belongs to a new stream. If this condition holds for multiple streams, then a collision occurs. We refer to such collisions as *slot collisions*.[4] We will analyze the collision probability in § 4.2.

When rise edges overlap (Figure 7), it is hard to separate them. As a result, they are assigned to one stream and other streams miss pulses in certain symbols. Prior work [30] use the phase information to resolve edge collisions. This method, however, is not applicable here, since LEDs are incoherent light sources [21] and light signals do not own phase information. We solve this problem by buffering the most promising candidate rise edge (i.e., with the smallest rise edge offset) within the coming symbol. If no rise edge is assigned to a stream at the end of its symbol, then the rise edge is assumed to overlap with other rise edges and we decode the symbol using the most promising candidate. Because the rise edge offset with the correct rise edge is very small compared to L, we can still decode the symbol correctly. But we do not use this edge for future edge classification and stick to the former edge assigned to the stream.

4.2 Addressing Remaining Collisions

A DarkLight receiver can leverage Algorithm 1 to decode bits from multiple LEDs – let them be synchronous or unsynchronized. If the LEDs are synchronized, we can pre-allocate the slot beginnings evenly such that the rise edges can always be differentiated. With slot slot width L and rise edge offset range $\theta(<< L)$, each DarkLight receiver can separate maximally $\lfloor L/\theta \rfloor$ LEDs. If the LEDs transmit in a laissez-faire fashion, it is possible that the slot offset of two pulse streams is within the rise edge offset range $[\underline{\theta}, \bar{\theta}]$, resulting into slot collisions and making our mechanism unable to separate them. Next we analyze the probability of slot collisions

[4]Note that the collision of two pulse streams does not affect the decoding of other streams that do not collide. Thus, we can let the collided streams re-transmit data without affecting other streams.

Algorithm 1: Identify the source of a new rise edge.

input : 1) t, start time of the rise edge to be classified;
2) $T[i]$, start time of the most recent rise edge of stream i;
3) L: time slot width;
4) $[\underline{\theta}, \bar{\theta}]$, rise edge offset range.
output: s, the stream number that the new rise edge is classified to.

```
n = 0                                          /* # of streams */
cnt = 0
k = 0
for i ← 1 to n do
    m_i = round((t − T[i]) / F_s)              /* closest integer */
    q_i = t − m_i × F_s
    if (q_i > θ_) AND (q_i < θ̄) then
        cnt = cnt + 1
        k = i
    end
end
if cnt == 0                                    /* new stream */
then
    n = n + 1
    T[n] = t
    s = n
end
else if cnt > 1 then  s = −1                   /* collision */

else  T[k] = t;   s = k;                       /* existing stream */
```

with unsynchronized LEDs and leverage the analysis to fine-tune single DarkLight link configuration.

Analyzing Collision Probability. Assume N unsynchronized DarkLight transmitters that randomly start their transmissions[5], L is their slot width and θ is the width of the rise edge offset range, we have the following theorem on the probability of slot collisions.

THEOREM 1. *For $N(< \lfloor L/\theta \rfloor)$ unsynchronized DarkLight transmitters perceived by a DarkLight receiver, the probability p of slot collision (i.e., the time slot offset of two transmitters is shorter than θ) is*

$$p = 1 - (\frac{L - N \cdot \theta}{L})^{N-1}. \quad (1)$$

PROOF. Consider a DarkLight transmitter starting the transmissions and then the other $(N-1)$ transmitters choose the start times of their time slots within the slot of the first transmitter. A slot collision occurs when any two start times are less than θ away. Thus, we can translate the problem into the following: if we randomly put $(N-1)$ points into a line segment of length L, what is the probability p' of the resulting N line segments all longer than θ?

To derive p', let x_i denote the coordinate of the ith point. Then the sample space is

$$0 < x_i < L, \quad \forall i \in [1, N-1].$$

The volume V of the sample space is L^{N-1}, because it is a $(N-1)$-dimensional cube. On the other hand, the event space (i.e., all line segments are longer than θ) is

$$|x_i - x_j| > \theta \qquad \forall i \neq j, i, j \in [1, N-1]$$
$$\theta < x_i < L - \theta \qquad \forall i \in [1, N-1]$$

[5]In our design, if a packet follows the previous packet sufficiently close (less than a packet duration), we align its slots with the previous packet to reduce collision probability, because otherwise both packets can collide independently with a packet from another LED.

As we show in the Appendix, the volume V_E of the event space is $(L - N \cdot \theta)^{N-1}$. Therefore, we have $p' = \frac{V_E}{V} = (\frac{L - N \cdot \theta}{L})^{N-1}$, and the probability of slot collision is $1 - p'$, i.e., $1 - (\frac{L - N \cdot \theta}{L})^{N-1}$. □

Eq. (1) indicates that slot collisions are less likely to occur with larger time slot width L. A larger L, however, leads to fewer time slots per symbol and thus fewer bits encoded per pulse, as shown in § 3.2. Next we describe how to judiciously configure L to take into account the network condition and achieve the best tradeoff.

Configuring Time Slot Width L. Based on the collision probability derived in Theorem 1, we can now compute the expected throughput for each DarkLight link as well as the whole network. This allows us to properly configure the time slot width L to optimize link performance taking into account the network condition (i.e., LED density, receiver photodiode's FoV). We discuss two possible objective functions that we can optimize through configuring L.

First, for applications prioritizing throughput, we can configure L to maximize the expected link throughput. Based on the LED density and receiver photodiode's FoV, we can estimate the number of LEDs N that a receiver can perceive. Based on Theorem 1, the probability that a DarkLight link does not collide with others is $(\frac{L - 2\theta}{L})^{N-1}$. A single link's throughput without any collision is $\frac{\log_2 t_{\text{symbol}}/L}{t_{\text{symbol}}}$. Thus, the expected throughput $\mathbb{E}[Y]$ of a single transmitter is

$$\mathbb{E}[Y] = \frac{\log_2 (t_{\text{symbol}}/L)}{t_{\text{symbol}}} \cdot (\frac{L - 2\theta}{L})^{N-1}. \quad (2)$$

By setting $\frac{d\mathbb{E}[Y]}{dL} = 0$, we can numerically derive the optimal slot width L^* such that $\frac{d\mathbb{E}[Y(L^*)]}{dL} = 0$.

Second, for applications that prioritize reliability, we can configure L to ensure that the collision probability p is below δ while maximizing the link data rate. By setting $(1 - (\frac{L - N \cdot \theta}{L})^{N-1}) = \delta$, we can derive the optimal L^* as:

$$L^* = \frac{N \cdot \theta}{1 - (1 - \delta)^{\frac{1}{N-1}}}. \quad (3)$$

Similarly, if only a specific link needs to be highly reliable, we can configure L to ensure the collision probability of a single link is below a threshold δ, by setting $(1 - (\frac{L - 2\theta}{L})^{N-1}) = \delta$ to derive the $L^* = \frac{2\theta}{1 - (1-\delta)^{\frac{1}{N-1}}}$.

The benefit of the above slot configuration depends on the traffic pattern. If the traffic occurs so sparsely that only one LED transmits data most of the time, a shorter slot results in higher throughput. However, when the traffic is heavy (e.g., ceiling LED's downlink traffic), or when concurrent transmissions are required (e.g., sensing applications), simple retransmission causes frequent collisions, leading to lower network throughput and higher latency. Configuring L is advantageous by reducing collisions in the first place.

5. DarkLight PROTOTYPE

We build DarkLight prototype following the circuit design in § 3.1. Figure 8 and 9 show the complete circuit for DarkLight transmitter and receiver. In § 6.2, we will measure the power consumption of the circuit.

Transmitter. We use off-the-shelf LEDs (integrated array chip-on-board) targeted for indoor illumination. We have tested different models from different manufacturers and they have shown similar timing characteristics. The prices range from $7 to $17. In our prototype, the default LED is Cree CXA 2520. We implement the

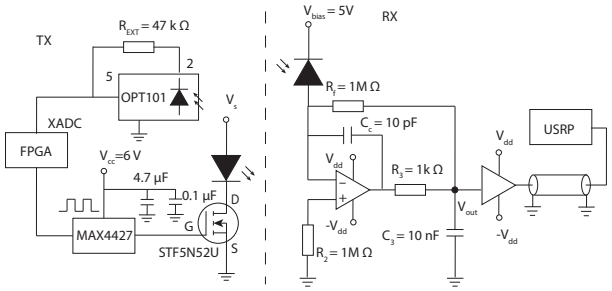

Figure 8: The circuit design of DarkLight.

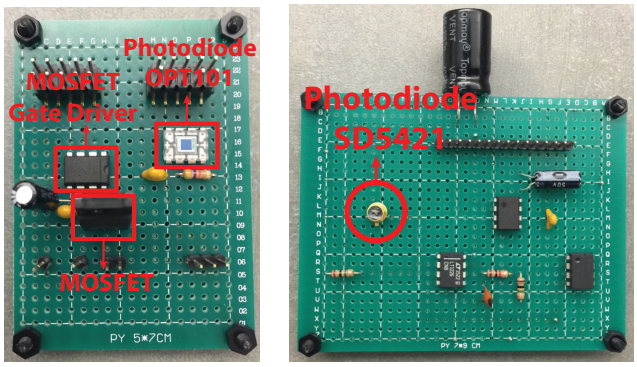

(a) Transmitter (b) Receiver

Figure 9: Implementation of DarkLight transmitter and receiver on general-purpose PCBs.

TX physical layer on an FPGA. We choose FPGAs because they can generate ultra-short pulses and control the pulse positions at the clock-level granularity required by OPPM. We use the Basys 3 FPGA board equipped with a Xilinx Artix-7 FPGA ($79). Its clock speed is 100 MHz, but due to the constraint of the GPIO, the shortest output pulse is 40 ns.

To implement the adaptation described in § 3.3, we equip the LED with a photodiode OPT101 ($8) with on-chip transimpedance amplifier. The internal feedback resistor (1 MΩ) of OPT101 is too large to measure ambient light intensity because it easily saturates. Thus we connect it to an external 47 kΩ feedback resistor to ensure that it can measure strong ambient light. We sample the output of OPT101 using the built-in 12-bit 1MS/s Analog-to-Digital Converter (ADC) on Artix 7. The FPGA samples data from the photodiode every 5 seconds[6], estimates the current ambient light condition, and then configures the LED duty cycle based on Table 1. We adapt the duty cycle exponentially in base 2, so that the number of slots per symbol remains a power of 2 across all ambient light levels, which ensures efficient data encoding.

Receiver. The receiver photodiode is Honeywell SD5421 ($6) and its shortest response time is 15 ns. To support a reasonable distance, we use a 1 MΩ feedback resistor in the transimpedance amplifier. It increases the gain and yet also prolongs the received light pulse width from 500 ns to 40 μs. The prolonged pulse width has a minimal impact since we rely only on the rise edge of the light pulse to encode/decode bits. We sample light signals using a USRP N200 with an LFRX daughterboard and between the output signal and USRP is a voltage follower to prevent the low input impedance of LFRX from loading the signal. We use USRP in our prototype for research purpose, since it can support sampling rates up to 25 MS/s (lower than its capacity 100 MS/s due to the Ethernet connection between USRP and PC), allowing us to evaluate a wide range of sampling rates. In practical usage scenarios, the sampling rate can be much lower. Thus USRP is not necessarily needed and can be replaced with low-power FPGAs. We implement the RX physical layer using GNU radio with C++.

[6]To minimize the impact of sensor data noise, the FPGA fetches 1024 samples each time and computes the average. The sensing duration is 1.024 ms in total.

Table 1: The mapping table for DarkLight to adapt LED's duty cycle to the current ambient light condition.

Ambient illuminance	LED duty cycle	# bits per symbol
$<$ 600 lx	0.0076%	10
600 lx–1200 lx	0.015%	9
$>$ 1200 lx	0.031%	8

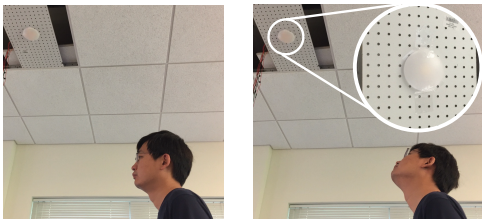

(a) Indirect viewing (b) Direct viewing

Figure 10: Two viewing scenarios in DarkLight's user perception study (§ 6.1). In indirect viewing (a), the user naturally looks around the environment, while in direct viewing (b), the user directly stares at the DarkLight transmitter with a lampshade.

6. DarkLight EVALUATION

We evaluate DarkLight by examining two aspects: 1) *user perception*: whether users actually perceive the ultra-low luminance from DarkLight transmitters under varying ambient light conditions, and 2) *system performance*: DarkLight's throughput under varying distances and viewing angles, power consumption, and its multi-link throughput.

Experiment Setup. We use the prototype described in § 5. By default, we set pulse width t_{ON} as 500 ns, the time slot width L as 3.2 μs, and the symbol length t_{symbol} as 6.55 ms. The DarkLight receiver is placed right under the transmitter at 1.3-m distance. The receiver samples light signals using a USRP with 1 MS/s sampling rate and decodes data. We then calculate throughput (i.e., the number of bits correctly received) and accuracy (i.e., percentage of bits correctly received) as our performance metrics. All experiments are repeated for five rounds.

6.1 User Perception

We conduct a user study[7] to systematically examine user's perception of the ultra-short light pulses from a DarkLight LED. We recruit 20 participants (13 male and 7 female) between 22 to 60 years old. We mount a DarkLight LED with a lampshade on an office ceiling (2.6 m in height, Figure 10). We examine whether participants can distinguish a DarkLight LED and an LED that is actually off. We randomly switch the LED between the light-off mode and the DarkLight mode with different duty cycles (pulse width 500 ns). Participants are not aware of LED's actual state. For each trial, users select whether they believe the light is on or off. For each LED state, which appears three times, we calculate how likely users perceive the LED off by the ratio $R_{\text{off}} = \frac{N_{\text{OFF}}}{N_{\text{ON}}+N_{\text{OFF}}}$,

[7]We have obtained the IRB approval at our local institution for the user study.

Table 2: User perception of DarkLight in indirect viewing. The percentage (R_{off}) is the likelihood of users perceiving the LED to be off.

Duty cycle	Ambient light level				
	1	2	3	4	5
light off (0.05 lx)	97%	93%	95%	87%	100%
0.0067% (0.06 lx)	97%	93%	93%	92%	65%
0.018% (0.07 lx)	95%	97%	98%	82%	82%
0.047% (0.101 lx)	95%	92%	95%	87%	60%
0.13% (0.191 lx)	97%	93%	95%	83%	45%
0.33% (0.412 lx)	98%	97%	93%	80%	17%
0.88 % (1.06 lx)	93%	93%	88%	80%	12%
2.3% (2.78 lx)	83%	87%	82%	50%	2%
6.25% (7.4 lx)	92%	90%	83%	18%	0%

Table 3: User perception of DarkLight in direct viewing.

Duty cycle	Ambient light level				
	1	2	3	4	5
light off (0.04 lx)	83%	95%	98%	98%	90%
0.0025% (0.05 lx)	88%	82%	67%	13%	2%
0.0035% (0.05 lx)	90%	80%	42%	12%	2%
0.005% (0.05 lx)	68%	70%	35%	5%	0%
0.0071% (0.05 lx)	80%	37%	18%	3%	0%
0.01% (0.06 lx)	73%	33%	13%	3%	0%
0.014% (0.06 lx)	65%	8%	5%	7%	0%

where N_{OFF} and N_{ON} are the number of times that participants think the LED is off and on respectively.

As shown in Figure 10, we instruct users to view the LED in two manners: 1) indirect viewing, where participants look at the environment and make their judgments by perceiving the illuminance on walls, floor, and other objects in the room; and 2) direct viewing, where participants raise their heads and stare at the ceiling LED directly. The distance between user eyes and the LED is within 0.7 – 1 m. Indirect viewing is our primary target scenario since it is the more natural way we perceive ceiling LEDs in our daily life.

We conduct the experiment in five different ambient light conditions: (1) 550 lx–600 lx (e.g. a sunny day with fluorescent lights on); (2) 100 lx–150 lx (e.g. a sunny day with other artificial lights off); (3) 30 lx–50 lx (e.g. afternoon to dusk with other artificial lights off); (4) 2 lx–12 lx (e.g. afternoon to dusk with all window blinds down); (5) 0.01 lx–0.05 lx (e.g. on a clear night or in a completely dark room with windows covered by thick curtains).

Table 2 and Table 3 summarize the results in these two viewing settings, respectively. In the first column, we also include the illuminance measured at night incurred by the LED at 1-m distance for each LED duty cycle. An interesting note is that the R_{off} ratio is not always 1 even for the light-off mode, indicating the sophistication of human vision perception under varying ambient light levels. Thus the difference in the R_{off} value between DarkLight and light-off mode better indicates how well DarkLight performs in hiding light pulses. We make three key observations. *First*, in the indirect viewing scenario, our default LED duty cycle setting (0.007%) allows the DarkLight LED to be perceived very similar ($< 7\%$ difference in R_{off}) to an LED in the actual light-off mode. It demonstrates the efficacy of DarkLight's design principle. *Second*, ambient light levels greatly affect human perception of light. In a bright condition (ambient light level 1), a duty cycle of 0.33% allows DarkLight LED to be indistinguishable from the light-off mode, whereas in the dark night (ambient light level 5) the duty cycle needs to be under 0.007% for DarkLight LED to be similar to actual light-off mode. This result indicates the necessity of LED duty cycle adaptation (§ 3.3). *Third*, direct viewing is a much more challenging scenario as more photons enter human eyes. As a result, it requires a lower duty cycle (e.g., 0.0025%) to keep DarkLight similar to the light-off mode in the day (ambient light level 1 - 3). In the night, human eyes are sensitive to photons and can perceive the DarkLight LED in direct viewing. Note that this is an extreme viewing scenario for ceiling LEDs. Direct viewing is more natural when applying DarkLight to mobile devices for short-range (e.g., 10 cm) communication, where we can configure a shorter pulse width (e.g., 100 ns) to better keep light pulses imperceptible.

Table 4: User perception (R_{off}) of DarkLight: 5 LEDs v.s. 1 LED.

Duty cycle (x)	5 LEDs	1 LED	Duty cycle ($5x$)
0.0025%	87%	67%	0.0125%
0.0035%	67%	60%	0.0177%
0.0050%	93%	40%	0.0250%
0.0071%	87%	27%	0.0354%
0.0100%	73%	20%	0.0500%
0.0141%	60%	0%	0.0707%

Spatial Density. After examining user's perception of a single DarkLight LED, we next evaluate the perception of multiple DarkLight LEDs. We seek to understand whether the illuminance from m DarkLight LEDs is perceived the same as a single LED emitting the equal amount of illumiance with a duty cycle m times higher. To this end, we test two scenarios as below: (1) 5 DarkLight LEDs (4 placed in a 7 cm $\times$ 7 cm square and 1 in the square center) each with a duty cycle of x, and (2) one LED with a duty cycle of $5x$. We conduct the user study with 5 participants in the direct viewing scenario, where the ambient illuminance is 564 lx. Table 4 compares the R_{off} ratios as LED duty cycle x varies. Our key observation is that users are much less likely to perceive light in scenario (1). This is because the same amount of optical energy is spatially spread out in scenario (1), making human eyes less sensitive [20]. Furthermore, users perceive 5 DarkLight LEDs (0.0141%) almost the same as a single LED operating with a similar duty cycle (0.0177%), because of the similar spatial density of optical energy. It demonstrates that scaling out DarkLight LEDs does not lose the imperceptibility.

Flickering Effect. We also examine whether DarkLight causes any flickering effect because of its long period (6.56 ms). In our implementation, the lowest flashing rate is approximately 160 Hz. In the user study, we ask users whether they perceive noticeable flickering. No user has reported any unless he/she stares at the LED at a very close distance (10 cm). The reason is that the minimal flashing rate to avoid flickering depends on the light intensity: the lower the light intensity, the lower the threshold [49]. Thus, although the lowest flashing rate of DarkLight is close to the threshold to avoid flickering for normal VLC, users do not perceive flickering in DarkLight.

6.2 Single-Link Performance

We now examine the performance of a single DarkLight link, focusing on the impact of different practical factors on its throughput. We also examine the power consumption of both the LED front end and driving circuits.

Throughput. We start with testing DarkLight's throughput at the default distance (1.3 m). Given that the time slot width L is a key parameter in DarkLight modulation (§ 3.2), we vary L under the default LED duty cycle to examine its impact on link throughput. We test three slot widths: 800 ns, 1600 ns, and 3200 ns, translating to 13, 12, and 11 bits encoded per symbol (6.56 ms), respectively. We transmit 1000 random bits each time and configure the RX with different sampling rates to measure the resulting throughput.

From Figure 11(a), we observe that DarkLight achieves 1.6 - 1.8 Kbps overall throughput once the sampling rate is sufficient to support a given time slot width. As expected, short time slots demand

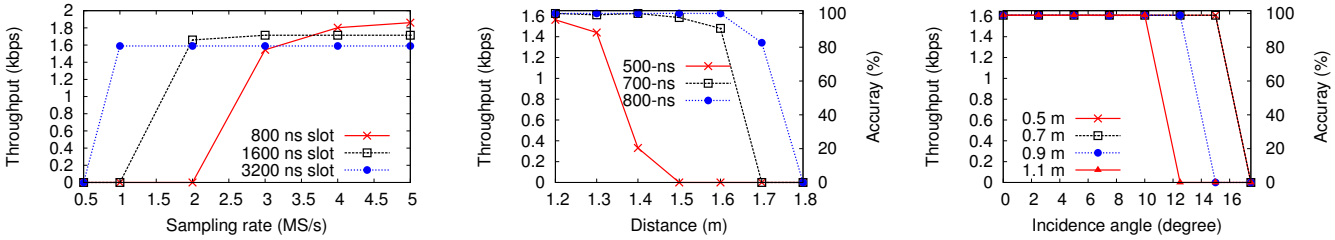

(a) Throughput w/ different time slot widths (b) Distance w/ different pulse widths (c) Viewing angle w/ different distances

Figure 11: DarkLight single-link performance.

higher sampling rates to detect rise edges correctly. When the sampling rate is not sufficiently high, the time interval between adjacent samples is too large, making the receiver fail to detect the preamble correctly and discard the whole packet. The result also indicates the lower-bound of L for a given sampling rate. For example, for the sampling rate of 1 MS/s, L needs to be above 1.6 μs, because the rise edge offset is already [-1 μs, 1 μs] with 2 μs range (Figure 6). In addition, reducing the slot width from 3.2 μs to 800 ns leads to marginal improvement in the throughput, because reducing the slot by half adds only 1 bit encoded per symbol. Since shorter time slots require higher sampling rates and higher power consumption, a 3.2-μs time slot achieves the best tradeoff in our current setting.

Supporting Distance. We now evaluate DarkLight's supporting distance. We measure DarkLight's throughput and accuracy as we vary the link distance from 1.2 m to 1.8 m. We test three pulse widths (500 ns, 700 ns, 800 ns). We place the receiver photodiode right below the LED with zero offset. Figure 11(b) shows that the default pulse width (500 ns) supports up to 1.3-m distance while maintaining 1.6-Kbps data rate. The throughput drops quickly to zero after the supporting distance, because the light intensity drops to the same level as circuit noise, making the receiver unable to detect any rise edge. A wider pulse width supports longer distances because a longer pulse duration allows the LED to ascend to a higher light intensity before LED reaches its peak. In practice, we set the pulse width based on the target distance in different application scenarios. From our experiments, we also observe that adding the lampshade decreases the supporting distance by approximately 30 cm. In office settings, human hands are typically 1.5 m away from the ceiling and thus 700–800 ns pulse width is sufficient.

Viewing Angle. Next we test DarkLight's robustness against receiver misalignment given the FoV of the LED and receiver photodiode. We move the receiver photodiode with different incidence angles while keeping the photodiode upward at a fixed distance to the LED. For each incidence angle, we measure the resulting throughput and accuracy at the receiver. Figure 11(c) plots the results for different link distances (0.5 m – 1.1 m). Our first observation is that the maximum viewing angle starts to decrease when the distance is longer than 0.9 m. This is because at shorter distances, the incidence angle dominates the degradation of the light intensity, while at longer distances, the distance dominates the degradation. Another observation is that that DarkLight is more robust against misalignments under longer link distances. For example, the coverage radius at 0.5 m is 12.9 cm (0.5 m$\times \sin 15^\circ$), while at 1.1 m is 19.1 cm (1.1 m$\times \sin 10^\circ$). This is because light beam propagates more widely as it travels further in a cone shape and thus the same offset distance results into smaller incidence angle thus smaller degradation in light intensity even at longer distances. The viewing angle of our current prototype, approximately 15°, is mainly limited by the FoV (18°) of the receiver photodiode (SD5421), which has a lens to focus light for higher gain.

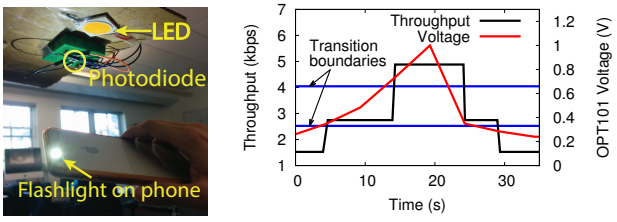

(a) Setup (b) Adaptation

Figure 12: Examine DarkLight's ability to adapt LED duty cycle to current ambient light condition. We systematically control a phone's flash light to emulate ambient light changes (a). DarkLight periodically (every 5 s) senses the ambient light using a photodiode next to the LED and adjusts its duty cycle and thus the data rate within 5 s delay.

Adaptation. Next we examine DarkLight's adaptiveness to ambient light fluctuations. We emulate ambient light change using a smartphone flashlight (Figure 12(a)). We use a commercial light meter (EXTECH 401036) to map the photodiode's voltage reading to the sensed illuminance, based on which the DarkLight LED adapts its current data rate. Figure 12(b) plots photodiode's voltage readings and the instantaneous throughput at the receiver, as the flashlight is moving towards and then away from the LED. The horizontal lines mark the voltage levels for transitioning to another data rate according to Table 1. We observe that DarkLight gracefully adapts its data rate as ambient light varies. The adaptation delay is within 5 seconds, because the FPGA fetches photodiode's data every 5 seconds (§ 5).

Power Consumption. DarkLight's power consumption comes from the LED front end and the driving circuits at both the transmitter and receiver. We measure the power consumption of the driving circuits as follows. For the FPGA, we estimate its post-routing power consumption using the power analysis tool provided in Xilinx Vivado. For each circuit component, we measure its power by $P = VI$. We connect a high-power, accurate 1-Ω resistor in series to each positive power rail (e.g. V_{dd}) and measure the voltage drop across the resistor using a digital multimeter. It allows us to obtain the current from the power supply. If the power supply is single-voltage supply, we use $P = V_{dd}I_{supply}$; if it is dual-voltage supply (e.g. $\pm$2.5 V), we use $P = 2V_{dd}I_{supply}$. When the current is too small (< 0.1 mA) with the resulting voltage (< 0.1 mV) across the resistor beyond voltage meter's resolution, we directly measure the current using the current meter. For the MOSFET gate driver, its power dissipation is $P = C_{\text{load}}V_{cc}^2 f$, where C_{load} includes the capacitance of the load (i.e., the input capacitance of the MOSFET, 529 pF) and the parasitic capacitance of the wiring from the gate

Table 5: Power consumption of each component in the driving circuit of the transmitter and receiver.

Transmitter			Receiver		
FPGA	MOSFET gate driver	PD (OPT101)	PD (SD5421)	transimpedance amplifier	voltage follower
78 mW	15–30 μW	$<$ 425 μW	$<$ 0.5 μW	45 mW	4.5 mW

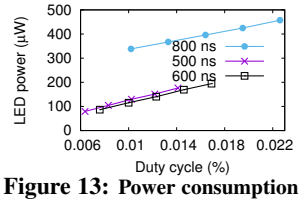

Figure 13: Power consumption of the LED front end under different LED duty cycles and pulse widths.

Table 6: Energy efficiency of DarkLight and normal VLC transmitters

	DarkLight	Normal VLC
Modulation	2048-OPPM	OOK
LED	104 μW	324 mW
Driver	15 μW	58.5 mW
PD (TX)	425 μW	–
Total power	544 μW	383 mW
Throughput	1.6 kbps	156 kbps
Efficiency	0.34 μJ/b	2.5 μJ/b

driver to the MOSFET, V_{cc} is 6 V (Figure 8), and f is the switching frequency. Note that we switch only once per symbol, so we need to multiply the frequency of the light pulse by the duty cycle. Because we are unable to measure the parasitic capacitance of the wiring, we stick to the $P = VI$ estimation. We measure 5 duty cycles from 0.0064% to 0.014% and 3 pulse widths (500 ns, 600 ns, 800 ns). The receiver's power consumption, based on our measurement, does not change with LED duty cycle.

Table 5 summarizes the power consumption of different circuit components. Overall, the driving circuits are very energy-efficient, with power consumption below 78 mW for the transmitter and 50 mW for the receiver, where the FPGA and the transimpedance amplifier dominate the power consumption. We can further lower the power by replacing the FPGA with ASIC.

Figure 13 plots the power consumption of the LED front end as its duty cycle increases under different pulse widths. As expected, given a pulse width, the LED power increases linearly with the duty cycle. Yet with the small duty cycles used in DarkLight, the LED power stays below 500 μW, several orders of magnitude lower than its normal power (19.8 W). Given a duty cycle, a longer pulse width leads to higher energy consumed in the ON duration, thus 800-ns pulses leads to higher power. However, a longer pulse also entails a longer symbol length to maintain a given duty cycle, which compensates the increase in the pulse energy. Thus 600-ns pulses consume slightly lower power than that of 500 ns.

We further compare DarkLight's energy footprint to normal VLC, using the metric of energy consumption per bit (Joule/b). To eliminate the discrepancy in hardware implementation, we implement normal VLC on the same DarkLight prototype by increasing its duty cycle to 8% while fixing the pulse duration. Table 6 summarizes the comparison. We observe that DarkLight consumes only 13.6% of normal VLC's energy to transfer one bit, because of its encoding efficiency (encoding 10x more bits per light pulse than OOK) and its low-power circuit design. While normal VLC can boost data rates using advanced modulation schemes such as OFDM, these modulation schemes require higher-end driving circuit with higher energy cost. To the best of our knowledge, no prior work has measured the circuit energy overhead of OFDM VLC systems, so no detailed comparison can be made. Since the power of IR emitters (100 mW to 20 W [1, 2, 4, 6]) is similar to that of LEDs, we expect DarkLight achieves similar energy gains over IR.

6.3 Multi-Link Performance

Finally we evaluate DarkLight's performance when multiple links are present. Because of the high directionality of light propagation and the limited viewing angles (FoV) of photodiodes, a VLC network inherently allows dense concurrent links transmitting data successfully and a DarkLight network is no exception. However, in a small local region, light signals within a photodiode's FoV can still collide and interfere with one another. Our multi-link experiments aim to examine how a DarkLight receiver deals with multiple perceived DarkLight LEDs, using the design in § 4.

Synchronized LEDs. We first examine scenarios with synchronized LEDs (e.g., ceiling LEDs all centrally controlled), where we set up 20 DarkLight LEDs in a 0.3 m $\times$ 0.2 m (0.06 m^2) rectangle area (Figure 14(a)) to emulate a local conflict zone in the DarkLight network. These LEDs are centrally controlled by an FPGA. We instantiate multiple DarkLight modules on the FPGA and create a top control module to allocate the start times of these LEDs' time slots. It ensures that the start times of LEDs' time slots are spread out without any two less than L/N away, where L is slot width and N is the transmitter number. We gradually switch on LEDs to increase the number of transmitters. For each given number of LEDs, we configure L to the optimal L^* that allows the receiver to receive packets from all transmitters successfully.[8]

Figure 14(b) plots the receiver's throughput as the number of perceived LEDs increases. We observe that the throughput at a single receiver increases almost linearly with the number of LEDs. It demonstrates the efficacy of DarkLight's design in dealing with interfering transmitters. The marginal gain decreases as the number of LEDs grows. It is because that when we increase LEDs, for a given sampling rate and symbol length, we need to extend the slot width to make sure the rise edges from multiple LEDs are distinguishable. So the number of bits encoded per symbol decreases for all LEDs. The implication behind the throughput gain provided by LED number is that we increase the pulse density and naturally it will increase the added optical transmit power, thus added luminance. But it is different from increasing the duty cycle of a single link because the emitted photons are spread out, resulting into multiple line-of-sight paths, which can be valuable for visible light sensing applications.

Unsynchronized LEDs. We next examine scenarios with unsynchronized LEDs (e.g., DarkLight used in mobile devices in a peer-to-peer manner, or in diverse surrounding asynchronous lights for light sensing [39, 52]), where LEDs start their transmissions without any coordination. Specifically, we test the worst-case scenario, where for all LEDs within the viewing angle of a receiver's photodiode, their packets overlap. We use the same LED layout shown in Figure 14(a) and configure[9] L based on the slot configuration in § 4.2. Each transmitter selects a random slot offset (the random numbers are generated beforehand and stored in the FPGA's ROM) with respect to its previous packet slots. An LED transmits 100 packets continuously in each round of experiment. In Figure 14(b), we plot the network throughput as the number of LEDs increases to 20. We observe that network throughput is approximately half that of synchronized LEDs, mainly because longer slot width results in fewer bits encoded in each symbol and slot collision can corrupt decoding, which does not occur among synchronized LEDs.

We further validate the efficacy of the collision probability model and the slot configuration in § 4.2 by experimenting 5 LEDs. For a given number of LEDs, we log the packets correctly received and calculate the ratio of these packets, referred to as the *collision-free rate*. We repeat the experiment as we vary the slot width from

[8]For 2, 3, 4, 5, 10, 15, and 20 LEDs in a 0.06-m^2 area, the optimal L for synchronized LEDs is 12.8 μs, 12.8 μs, 25.6 μs, 25.6 μs, 51.2 μs, 51.2 μs, and 102.4 μs respectively.

[9]For 2, 3, 4, 5, 10, 15, and 20 LEDs in a 0.06-m^2 area, the optimal L for unsynchronized LEDs is 25.6 μs, 51.2 μs, 51.2 μs, 102.4 μs, 204.8 μs, 204.8 μs, and 204.8 μs respectively.

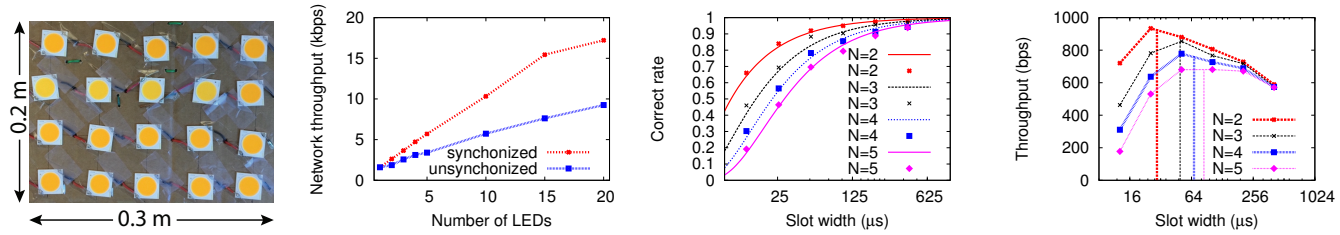

(a) Setup (b) Scalability (c) Unsynchronized Collision (d) Unsyncrhronized Throughput

Figure 14: DarkLight's multi-link experiments. LEDs are arranged as shown in (a). For a single receiver, its throughput scales linearly as the number of perceived LEDs increases (b). When LEDs' transmission is unsynchorized, the ratio of the collision-free packets over the transmitted fits the analytical model well. The markers represent experiment result and the lines represent the model (θ = 2.3 μs) in § 4.2 (c). For a fixed number of LEDs, an optimal configuration for slot width exists. The vertical lines represent the optimal slot width solved using the analytical model (§ 4.2) (d).

12.8 μs to 409.6 μs and increase the number of LEDs from 2 to 5. In Figure 14(c), we compare the measured collision-free rates indicated as markers to that derived by our model indicated by lines. The experimental results well align with the model, validating the model accuracy. We further examine whether the optimal slot width (L^*) derived from our model indeed leads to the highest throughput. In Figure 14(d), we plot the network throughput achieved by each slot width and mark L^* as vertical lines for different number of LEDs. We observe that L^* lies in very close proximity to the throughput peak in all cases. The small offset is due to the fact that in Eq. (2), the number of bits per symbol is not rounded to a number that is power of two. This is to ensure the expected throughput differentiable and we can optimize it conveniently. Overall the analytical L^* accurately reflects the actual throughput performance.

7. RELATED WORK

Low-Luminance VLC. Two prior works have studied a similar concept of DarkLight. In [17], Borogovac *et al* analyzed the achievable data rates in varying low illuminance levels. They leveraged optical channel models to derive SNRs and the theoretical data rates. Our work differs in that we present a complete system design to realize light communication in the dark. Another prior work is our preliminary study [48], where we demonstrated the feasibility of a single-link DarkLight using off-the-shelf LEDs and photodiodes, with a communication distance of 10 cm. In this work, we have greatly advanced the design, extended the supporting distance, and addressed the networking challenge in multi-link scenarios.

VLC Modulation. Active research has studied VLC modulation designs. We classify them into two categories: 1) basic single-carrier pulse modulation schemes that encode bits into pulse presence [43, 51], pulse width, pulse position [41, 44, 45], pulse amplitude, the light polarization [57], or color [29], and 2) advanced multi-carrier pulse modulation schemes (e.g., OFDM) that require more complicated hardware [21, 23]. In this work, we focus on single-carrier pulse modulation schemes for hardware simplicity. DarkLight's modulation design is inspired by prior schemes. It faces a new constraint of keeping light pulses imperceptible.

VLC Applications. Prior works [11, 26, 56, 58] have investigated using signal lights and car's headlights to enable road-to-vehicle and vehicle-to-vehicle communication and improve road safety. In addition to communication, other VLC applications include indoor localization and human sensing. VLC-based localization employs LEDs as anchors that broadcast beacons with light IDs and locations [35, 38]. A recent design [57] further allowed any light sources to be used for indoor localization. Aminikashani *et al* investigated positioning in OFDM-based VLC systems [10]. In [54], Xie *et al* proposed adding IDs to lights by covering each light with a coded lampshade that rotates around the LED. A recent work combined inertial and light sensors on smartphones for indoor localization without modulating the light [55]. Visible light sensing collects light intensity values from photodiodes and tracks bodies [39, 40] or finger movements [59]. All these systems can leverage DarkLight to broaden their sensing scenarios.

IR Communication. IR communication shares similarity with DarkLight, as it is also imperceptible and operates on optical channels. Prior works [8, 12, 18, 19, 25, 32, 33, 47] have extensively studied its modulation schemes using intensity modulation with direct detection (e.g., OOK, PPM, and subcarrier modulation), IR's channel characteristics, potential IR noise sources, MAC protocols, and designs of transmitters and receivers to maximize the link signal-to-noise ratios. However, these modulation schemes are designed for intrinsically imperceptible IR and cannot keep DarkLight's light pulses imperceptible.

8. CONCLUSION AND FUTURE WORK

We presented DarkLight, a new VLC primitive that allows light-based communication to be sustained even when LED lights appear dark or off. We tackled systems challenges to realize DarkLight using off-the-shelf, low-cost LEDs and photodiodes. We also systematically studied the networking challenges of DarkLight and enabled a DarkLight receiver to receive data from multiple transmitters simultaneously. We demonstrated the efficacy of our design using a DarkLight prototype, which achieves 1.6 Kbps with 1.3-m supporting distance. DarkLight pushes the limits of existing VLC designs, fundamentally broadens VLC's applicable scenarios, and provokes new thinkings on VLC applications.

Moving forward, we plan to advance DarkLight as follows. *First*, DarkLight's current data rate and communication range are mainly constrained by the response time of low-end LEDs and low-cost photodiodes. To boost DarkLight's data rate and range, we will explore higher-end LEDs and photodiodes to examine DarkLight's ultimate limit. We will also consider more advanced driving circuit designs such as pulse shaping techniques [14, 15, 16, 27] to generate shorter and higher light pulses. *Second*, we will improve DarkLight's energy efficiency. We use USRP in our current prototype to explore the impact of different sampling rate. For a given application, we can replace USRP with a dedicated ADC consuming lower power. Existing ADCs [5] supporting 2Msps sampling rate consume only 3.7 mW power. We also plan to implement the transmitter and receiver using ASIC [9] to further lower the power. *Third*, the principle of DarkLight can be applied to IR to lower IR

energy for eye safety. We will port our system to commercial IR emitters and examine its performance tradeoffs.

9. ACKNOWLEDGMENTS

We sincerely thank the reviewers for their insightful comments. We thank DartNets lab members for their support on our study. This work is supported in part by the National Science Foundation under grant CNS-1552924. Any opinions, findings, and conclusions or recommendations expressed in this material are those of the authors and do not necessarily reflect those of the funding agencies or others.

Appendix

We claim that the volume of the event space is $(L - N\theta)^{N-1}$. According symmetry, the event space consists of multiple parts of equal volume and in each part, the points have different oder. There are $(N-1)!$ possible orders so there are $(N-1)!$ number of parts. So we can calculate the volume of one part and then add them up. Without generality, let's assume

$$x_1 < x_2 < \ldots < x_{N-1}.$$

Then the part can be expressed as, elmimating the absolute value:

$$\begin{aligned} \theta < x_1 < L - (N-1)\theta\,, \\ x_1 + \theta < x_2 < L - (N-2)\theta\,, \\ \ldots \\ x_{N-2} + \theta < x_{N-1} < L - \theta\,. \end{aligned}$$

So the volume of the part can be calculated using the following integral:

$$V = \int_{\theta}^{L-(N-1)\theta} \int_{x_1+\theta}^{L-(N-2)\theta} \ldots \int_{x_{N-2}+\theta}^{L-\theta} 1\, dx_{N-1} \ldots dx_2\, dx_1$$

Let's substitute the variables by:

$$\begin{aligned} y_1 = x_1 - \theta\,, \\ y_2 = x_2 - 2\theta\,, \\ \ldots\,, \\ y_{N-1} = x_{N-1} - (N-1)\theta\,. \end{aligned}$$

Then,

$$\begin{aligned} & V \\ =& \int_0^{L-N\theta} \int_{y_1}^{L-N\theta} \ldots \int_{y_{N-2}}^{L-N\theta} 1\, dy_{N-1} \ldots dy_2\, dy_1 \\ =& \int_0^{L-N\theta} \ldots \int_{y_{N-3}}^{L-N\theta} (L - N\theta - y_{N-2})\, dy_{N-2} \ldots dy_1 \\ =& \int_0^{L-N\theta} \ldots \int_{y_{N-3}}^{L-N\theta} -(y_{N-2} - (L - Na))\, dy_{N-2} \ldots dy_1 \end{aligned}$$

We have

$$\begin{aligned} & \int_{y_{N-3}}^{L-N\theta} -(y_{N-2} - (L - N\theta))\, dy_{N-2} \\ =& -\frac{1}{2}(y_{N-2} - (L - N\theta))^2 \Big|_{y_{N-3}}^{L-N\theta} \\ =& \frac{1}{2}(y_{N-3} - (L - N\theta))^2\,. \end{aligned}$$

$$\begin{aligned} & V \\ =& \int_0^{L-N\theta} \ldots \int_{y_{N-4}}^{L-N\theta} \frac{1}{2}(y_{N-3} - (L - N\theta))^2\, dy_{N-3} \ldots dy_1 \\ =& \int_0^{L-N\theta} \ldots \int_{y_{N-5}}^{L-N\theta} -\frac{1}{2\cdot 3}(y_{N-4} - (L - N\theta))^3\, dy_{N-4} \ldots dy_1 \\ =& \ldots \\ =& \int_0^{L-N\theta} (-1)^{N-2} \frac{1}{(N-2)!}(y_1 - (L - N\theta))^{N-2} dy_1 \\ =& (-1)^{N-2} \frac{1}{(N-1)!}(y_1 - (L - N\theta))^{N-1} \Big|_0^{L-N\theta} \\ =& 0 - (-1)^{N-2} \frac{1}{(N-1)!}(0 - (L - N\theta))^{N-1} \\ =& (-1)^{2(N-1)} \frac{(L - N\theta)^{N-1}}{(N-1)!} \\ =& \frac{(L - N\theta)^{N-1}}{(N-1)!}\,. \end{aligned}$$

Therefore the volume of the original event space is

$$(N-1)! \cdot V = (L - N\theta)^{N-1}$$

10. REFERENCES

[1] 20w ir / infrared led 850nm high power led chips. http://www.ebay.com/itm/like/251460870814?lpid=82&chn=ps&ul_noapp=true.

[2] 5mm led - infrared (ir) 850nm 50 degree viewing angle. http://www.ledsupply.com/leds/5mm-led-infrared-850nm-50-degree-viewing-angle?gclid=Cj0KEQjwh428BRCnvcyI-5nqjY4BEiQAijebwj86FrCc82vt_6cqrz_V7ezL4qjOF7jVCikKhFX3sokaAhPb8P8HAQ.

[3] High Power Flash LED. http://www.samsung.com/global/business/business-images/led/file/product/it-c/201312/Data_Sheet_FH411B_SPFCW24301CL.pdf.

[4] High speed infrared emitting diodes, 940 nm, surface emitter technology. http://www.mouser.com/ds/2/427/vsmy2940rg-552474.pdf.

[5] MAX11102: 2Msps/3Msps, Low-Power, Serial 12-/10-/8-Bit ADCs. https://www.maximintegrated.com/en/products/analog/data-converters/analog-to-digital-converters/MAX11102.html.

[6] Oslon black series (850 nm). http://www.mouser.com/ds/2/311/SFH%204715A%20%20Lead%20(Pb)%20Free%20Product%20-%20RoHS%20Compliant-461047.pdf.

[7] The Physical Web. http://google.github.io/physical-web/.

[8] AKHAVAN, K., KAVEHRAD, M., AND JIVKOVA, S. High-speed power-efficient indoor wireless infrared communication using code combining. i. *IEEE Transactions on Communications 50*, 7 (2002), 1098–1109.

[9] AMARA, A., AMIEL, F., AND EA, T. FPGA vs. ASIC for low power applications. *Microelectronics Journal 37*, 8 (2006), 669–677.

[10] AMINIKASHANI, M., GU, W., AND KAVEHRAD, M. Indoor positioning in high speed ofdm visible light communications. *arXiv preprint arXiv:1505.01811* (2015).

[11] ARAI, S., YAMAZATO, T., OKADA, H., FUJII, T., AND YENDO, T. LED acquisition methods for image-sensor-based visible light communication. In *Opto-Electronics and Communications Conference (OECC), 2015* (2015), IEEE, pp. 1–3.

[12] ARVIN, F., SAMSUDIN, K., AND RAMLI, A. R. A short-range infrared communication for swarm mobile robots. In *2009 International Conference on Signal Processing Systems* (2009), IEEE, pp. 454–458.

[13] BAR-DAVID, I., AND KAPLAN, G. Information rates of photon-limited overlapping pulse position modulation channels. *IEEE Transactions on Information Theory 30*, 3 (May 1984), 455–464.

[14] BINH, P., RENUCCI, P., TRUONG, V., AND MARIE, X. Schottky-capacitance pulse-shaping circuit for high-speed light emitting diode operation. *Electronics letters 48*, 12 (2012), 1.

[15] BINH, P., TRONG, V., HUNG, D., RENUCCI, P., BALOCCHI, A., AND MARIE, X. Demonstration of 300 mbit/s free space optical link with commercial visible LED. In *New Circuits and Systems Conference (NEWCAS), 2013 IEEE 11th International* (2013), IEEE, pp. 1–3.

[16] BINH, P., TRONG, V., RENUCCI, P., AND MARIE, X. Improving OOK modulation rate of visible LED by peaking and carrier sweep-out effects using-schottky diodes-capacitance circuit. *Journal of Lightwave Technology 31*, 15 (2013), 2578–2583.

[17] BOROGOVAC, T., ET AL. "Lights-off" visible light communications. In *Proc. of Globecom Workshop on Optical Wireless Communications* (2011).

[18] CARRUTHER, J., AND KAHN, J. M. Angle diversity for nondirected wireless infrared communication. *IEEE Transactions on Communications 48*, 6 (2000), 960–969.

[19] CARRUTHERS, J. B., AND KAHN, J. M. Multiple-subcarrier modulation for nondirected wireless infrared communication. *Selected Areas in Communications, IEEE Journal on 14*, 3 (1996), 538–546.

[20] CORNSWEET, T. *Visual perception*. Academic press, 2012.

[21] DIMITROV, S., AND HAAS, H. *Principles of LED Light Communications: Towards Networked Li-Fi*. Cambridge University Press, 2015.

[22] FRANCO, S. *Design with operational amplifiers and analog integrated circuits*. McGraw-Hill, 2001.

[23] GHASSEMLOOY, Z., POPOOLA, W., AND RAJBHANDARI, S. *Optical wireless communications: system and channel modelling with Matlab®*. CRC Press, 2012.

[24] GRAEME, J. *Photodiode amplifiers: op amp solutions*. McGraw-Hill, Inc., 1995.

[25] GRINER, U. N., AND ARNON, S. Multiuser diffuse indoor wireless infrared communication using equalized synchronous cdma. *IEEE transactions on communications 54*, 9 (2006), 1654–1662.

[26] HAIDER, M., AND DONGRE, M. Vehicle to vehicle communication using visible light communication technology. In *Proceedings of 24th IRF International Conference* (2015), pp. 64–66.

[27] HALBRITTER, H., JÄGER, C., WEBER, R., SCHWIND, M., AND MÖLLMER, F. High-speed LED driver for ns-pulse switching of high-current leds. *IEEE Photonics Technology Letters 26*, 18 (2014), 1871–1873.

[28] HOROWITZ, P., HILL, W., AND HAYES, T. C. *The art of electronics*, vol. 2. Cambridge university press Cambridge, 1989.

[29] HU, P., PATHAK, P. H., FENG, X., FU, H., AND MOHAPATRA, P. Colorbars: Increasing data rate of led-to-camera communication using color shift keying. *Proceedings of the ACM CoNEXT* (2015), 1–12.

[30] HU, P., ZHANG, P., AND GANESAN, D. Laissez-faire: Fully asymmetric backscatter communication. In *Proc. of SIGCOMM* (2015).

[31] INTERSIL. *Eye Safety for Proximity Sensing Using Infrared Light-emitting Diodes*.

[32] JUNGNICKEL, V., POHL, V., NÖNNIG, S., AND VON HELMOLT, C. A physical model of the wireless infrared communication channel. *Selected Areas in Communications, IEEE Journal on 20*, 3 (2002), 631–640.

[33] KAHN, J. M., AND BARRY, J. R. Wireless infrared communications. *Proceedings of the IEEE 85*, 2 (1997), 265–298.

[34] KOMINE, T., AND NAKAGAWA, M. Integrated system of white LED visible-light communication and power-line communication. *IEEE Transactions on Consumer Electronics 49*, 1 (2003), 71–79.

[35] KUO, Y.-S., PANNUTO, P., HSIAO, K.-J., AND DUTTA, P. Luxapose: Indoor positioning with mobile phones and visible light. In *Proc. of MobiCom* (2014).

[36] LEE, T. Effect of junction capacitance on the rise time of led's and on the turn-on delay of injection lasers. *Bell System Technical Journal 54*, 1 (1975), 53–68.

[37] LI, J., ET AL. Retro-VLC: Enabling battery-free duplex visible light communication for mobile and IoT applications. In *Proc. of HotMobile* (2015).

[38] LI, L., HU, P., PENG, C., SHEN, G., AND ZHAO, F. Epsilon: A visible light based positioning system. In *Proc. of NSDI* (2014).

[39] LI, T., AN, C., TIAN, Z., CAMPBELL, A. T., AND ZHOU, X. Human sensing using visible light communication. In *Proc. of MobiCom* (2015).

[40] LI, T., LIU, Q., AND ZHOU, X. Practical Human Sensing in the Light. In *Proc. of MobiSys* (2016).

[41] NOSHAD, M., AND BRANDT-PEARCE, M. Expurgated PPM using symmetric balanced incomplete block designs. *Communications Letters, IEEE 16*, 7 (2012), 968–971.

[42] PALMER, S. E. *Vision science: Photons to phenomenology*, vol. 1. MIT press Cambridge, MA, 1999.

[43] SCHMID, S., ET AL. LED-to-LED visible light communication networks. In *Proc. of MobiHoc* (2013).

[44] SHIU, D.-S., AND KAHN, J. M. Differential pulse-position modulation for power-efficient optical communication. *Communications, IEEE Transactions on 47*, 8 (1999), 1201–1210.

[45] SUGIYAMA, H., AND NOSU, K. MPPM: a method for improving the band-utilization efficiency in optical PPM. *Lightwave Technology, Journal of 7*, 3 (1989), 465–472.

[46] SZELISKI, R. *Computer vision: algorithms and applications*. Springer Science & Business Media, 2010.

[47] TANG, A. P., KAHN, J. M., AND HO, K.-P. Wireless infrared communication links using multi-beam transmitters and imaging receivers. In *Communications, 1996. ICC'96, Conference Record, Converging Technologies for Tomorrow's Applications. 1996 IEEE International Conference on* (1996), vol. 1, IEEE, pp. 180–186.

[48] TIAN, Z., WRIGHT, K., AND ZHOU, X. Lighting Up the Internet of Things with DarkVLC. In *Proc. of HotMobile* (2016).

[49] TYLER, C. W., AND HAMER, R. D. Analysis of visual modulation sensitivity. iv. validity of the ferry–porter law. *JOSA A 7*, 4 (1990), 743–758.

[50] WANG, Q., GIUSTINIANO, D., AND GNAWALI, O. Low-cost, flexible and open platform for visible light communication networks. In *Proc. of HotWireless* (2015).

[51] WANG, Q., GIUSTINIANO, D., AND PUCCINELLI, D. OpenVLC: Software-defined visible light embedded networks. In *Proceedings of the 1st ACM MobiCom workshop on Visible light communication systems* (2014), ACM, pp. 15–20.

[52] WANT, R., HOPPER, A., FALCAO, V., AND GIBBONS, J. The active badge location system. *ACM Transactions on Information Systems (TOIS) 10*, 1 (1992), 91–102.

[53] WANT, R., SCHILIT, B., AND JENSON, S. Enabling the Internet of Things. *Computer 48*, 1 (Jan 2015), 28–35.

[54] XIE, B., TAN, G., AND HE, T. Spinlight: A high accuracy and robust light positioning system for indoor applications. In *Proceedings of the 13th ACM Conference on Embedded Networked Sensor Systems* (2015), ACM, pp. 211–223.

[55] XU, Q., ZHENG, R., AND HRANILOVIC, S. Idyll: indoor localization using inertial and light sensors on smartphones. In *Proceedings of the 2015 ACM International Joint Conference on Pervasive and Ubiquitous Computing* (2015), ACM, pp. 307–318.

[56] YAMAZATO, T., KINOSHITA, M., ARAI, S., SOUKE, E., YENDO, T., FUJII, T., KAMAKURA, K., AND OKADA, H.

Vehicle motion and pixel illumination modeling for image sensor based visible light communication. *IEEE Journal on Selected Areas in Communications 33*, 9 (2015), 1793–1805.

[57] YANG, Z., ET AL. Wearables can afford: Light-weight indoor positioning with visible light. In *Proc. of MobiSys* (2015).

[58] YOO, J.-H., JANG, J.-S., KWON, J., KIM, H.-C., SONG, D.-W., AND JUNG, S.-Y. Demonstration of vehicular visible light communication based on led headlamp. *International Journal of Automotive Technology 17*, 2 (2016), 347–352.

[59] ZHANG, C., TABOR, J., ZHANG, J., AND ZHANG, X. Extending mobile interaction through near-field visible light sensing. In *Proc. of MobiCom* (2015).